

Date of publication xxxx 00, 0000, date of current version xxxx 00, 0000.

Digital Object Identifier 10.1109/ACCESS.2017.Doi Number

# Traction Synchronous Homopolar Motor: Simplified Computation Technique and Experimental Validation

**Vladimir Dmitrievskii<sup>1</sup>, Vladimir Prakht<sup>1</sup>, Member, IEEE, Alecksey Anuchin<sup>2</sup>, Senior Member, IEEE, and Vadim Kazakbaev<sup>1</sup>**

<sup>1</sup>Department of Electrical Engineering and Electric Technology Systems, Ural Federal University, Yekaterinburg, 620002 Russia

<sup>2</sup>Department of Electric Drives, Moscow Power Engineering Institute, Moscow, 111250 Russia

Corresponding author: Alecksey Anuchin (e-mail: anuchinas@mpei.ru).

This research is supported by the Russian Science Foundation grant (Project No. 16-19-10618).

**ABSTRACT** The synchronous homopolar motor (SHM) has been attracting the attention of researchers for many decades. Various mathematical models of SHM have been proposed to deal with its complicated magnetic circuit. Among them, there are time-consuming 3D finite element models (FEM), equivalent circuit models neglecting some significant features of the machine design, and 2D FEM models with virtual excitation winding distorting magnetic field picture. This paper proposes a novel 2D FEM of SHM and shows that since there are no sources of excitation in the cross-sections of the rotor and stator stacks, no virtual elements are required. This model uses the general solution of the Gauss's law for magnetism containing excitation flux. The model is based on a set of magnetostatic boundary value problems for various rotor positions. The set of boundary problems is completed with the excitation equivalent circuit. The losses in the armature and field windings and in the stator and rotor magnetic cores are computed in postprocessing. All these computations are carried out for a single combination of stator and rotor stack. A symmetrization algorithm is proposed to extend the obtained results to the whole SHM. A comparison of the theoretical and experimental data for a nine-phase three-section 320 kW SHM is carried out. These SHMs were used in a mining truck with a carrying capacity of 90 tons.

**INDEX TERMS** AC machines, automotive applications, brushless motors, electric vehicles, electromagnetic modeling, mining industry, traction motor.

## I. INTRODUCTION

The synchronous homopolar motor (SHM) has been used in specific applications for over a century. The main advantage of the SHM is its simple and reliable construction with its brushless excitation located at the stator of the machine together with armature winding. SHMs are utilized as generators in traction applications [1], aircrafts and trains [2], welding inverters [3], [4], etc. Their use has been considered in kinetic energy storage systems [5] due to their ability to regulate flux. Moreover, in [6], [7] and [8], SHMs were used as traction motors. They can be utilized in high temperature and hazard environments as drives [9] and as high-power wind generators [10].

The SHM involves a complex configuration of the magnetic system, which is inconvenient for computation and optimization since magnetic flux changes its direction in three dimensions. In some parts of the motor, flux flows in

the axial direction, while in other parts, it flows in the transverse plane and changes its direction to the axial one when coming from laminated parts to the stator back iron or the magnetic sleeve on the rotor shaft. Therefore, the finite element model (FEM) in 3D was used to compute the operation points of these motors [1], [11], [12].

The experimental verification of the 3D FEM computation was performed in [11] for the 0.75 kW, 3600 rpm SHM. However, only a limited analysis was performed due to the huge complexity of computations. Flux linkages were computed for two configurations of the motor. The performance characteristics were evaluated in [12] using 3D FEM for the 10 kW, 24 krpm SHM with an external rotor configuration. However, no verification of the model and no computation time estimation were introduced. The SHM and wound rotor synchronous machine were compared in a low

power generation application in [1] using 3D FEM. Here, experimental validation was performed.

3D FEM ensures high accuracy but requires huge computation resources, which makes it nearly impossible to design and optimize the SHM using genetic algorithms or other optimization methods. Therefore, methods to simplify the computations using 2D models were introduced.

The virtual excitation coils were added to each rotor teeth in [1] and [13] in order to represent excitation flux in a 2D model. In the axial direction, the magnetic system was evaluated using analytical equations for the lumped parameters network. It was shown that the proposed approach can be used to estimate inductance and EMF in an idle mode of operation. Similar approaches and results were considered in [14].

The 2D FEM can be replaced with the detailed equivalent circuit. The equivalent magnetic circuit was developed for a low power synchronous homopolar generator in [5]. The advantage of this approach is the absence of the virtual excitation windings at the rotor teeth to simulate the impact of the field winding to the model. Thus, a tolerable match to the equivalent circuit method with 3D FEM is shown. However, the noticeable mismatch between methods appears in some motor parameter configurations.

The comparison of the efforts of the computation with 3D FEM and equivalent circuit models is investigated in [15] for the SHM. It was shown that the 3D FEM requires 10000 times more computation time than the equivalent circuit model. The satisfactory match of the results was obtained for an idle operation mode.

All of the examples considered above utilize SHM design with two stator rotor stack combinations (SRSCs). The papers [5], [14]–[15] consider 2D methods only for the idle operation mode and do not consider operation under load.

To summarize the review mentioned above, two kinds of FEM were proposed for the evaluation of the characteristics of the SHMs. The first is 3D FEM and the second is 2D FEM, where the axial and radial fluxes are evaluated using a magnetic circuit or FEM boundary value problems. The disadvantage of 3D FEM is the required computation resources, which makes it nearly impossible to optimize the electrical machine parameters. The disadvantage of the 2D FEM and equivalent circuits is their low accuracy: equivalent circuit models neglect details of the motor design, and 2D FEMs introduce the elements absent in reality, which distort the magnetic field picture in the motor.

This paper considers the 320 kW SHM of a 90-ton mining truck. A new approach to the 2D FEM is introduced, which helps to decrease computation time significantly compared to 3D FEMs and allows obtaining the needed parameters of machine operation. The obtained results are compared with the experimental results of a real nine-phase three-section 320 kW motor. The magnetic flux density in the transverse cross-section of the stacks is represented as two components: the excitation flux density (flux density of the magnetic

monopole distributed along the rotational axis) and the flux density of the armature winding. The computation area excludes the shaft and the rotor sleeves area; therefore, not only the flux density of the armature winding satisfies the law of magnetic charges absence (the Gauss's law for magnetism), but the monopole field does as well. The peculiarities of the monopole lie out of the computation area. Therefore, compared to known 2D FEMs, in the proposed 2D model, the computation area does not contain any imaginary elements and represents the magnetic field more correctly.

Also, the symmetry between electromagnetic processes in neighboring SRSCs is investigated in this paper, which allows predicting the torque and voltage waveforms of the whole motor by computing those for a single SRSC.

The proposed model is designed based on a magnetostatic approach with various rotor positions. For the given SHM, the SRSC symmetry has been studied to reduce the computation area and to determine the minimal range of the rotor position to be considered.

The losses in the rotor and stator cores are evaluated using postprocessing. The model allows evaluating the mechanical, active, and reactive powers, the torque waveform, etc.

## II. DESIGN FEATURES OF THE SHM

3D view of the SHM with three SRSCs mounted in the motor with spans between them is shown in Fig. 1. The stator stacks are mounted in the housing (back iron), and the rotor stacks are mounted on the sleeve fixed on the shaft. There are excitation windings in the spans between the SRSCs. In the slots of three stator stacks, there is a common twelve-pole armature winding (which is not shown in Fig. 1 to not clutter it and can be seen in Fig. 2b). The number of teeth of each rotor stack is equal to the number of the armature winding pole pairs,  $p = 6$ . Since the excitation windings create opposite poles in the adjacent rotor stacks, the side rotor stacks are rotated by 180 electrical (30 mechanical) degrees with respect to the middle rotor stack. The supply frequency is defined by the rotation speed as follows:  $f = p \cdot n/60$ . The electrical angular frequency and mechanical rotational speed are  $\omega = 2\pi f$ ;  $\Omega = 2\pi n/60$ , respectively.

The excitation magnetic flux of the middle SRSC divides in two fluxes and circuits through the side SRSCs. Therefore, the middle SRSC is twice as long as the ones on the sides.

The armature winding consists of three three-phase subwindings forming a nine-phase winding, each of which has its own neutral point. This is done in order to reduce the current in each phase to simplify the design of the traction inverter. The phase shift between adjacent phases is  $360^\circ/9 = 40$  electrical degrees. The phases are marked with digits from 0 to 8 as shown in Fig. 2a. The number of the stator slots  $Z_s$  is equal to 54. The number of the stator slots per 2 poles is equal to  $Z_s/p = 54/6 = 9$ . A two-layer winding with the coil pitch of four stator slots is used. The phase current is supposed to be sinusoidal.

The schematic diagram of the traction inverter for the SHM is shown in Fig. 3. The inverter contains three three-phase inverters and a separate chopper for the excitation current control.

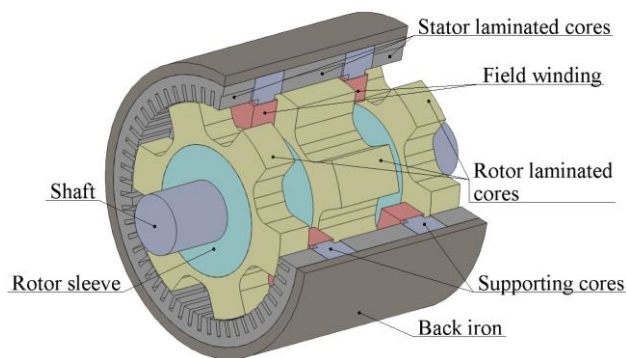


FIGURE 1. Sketch of the motor. Armature winding is not shown.

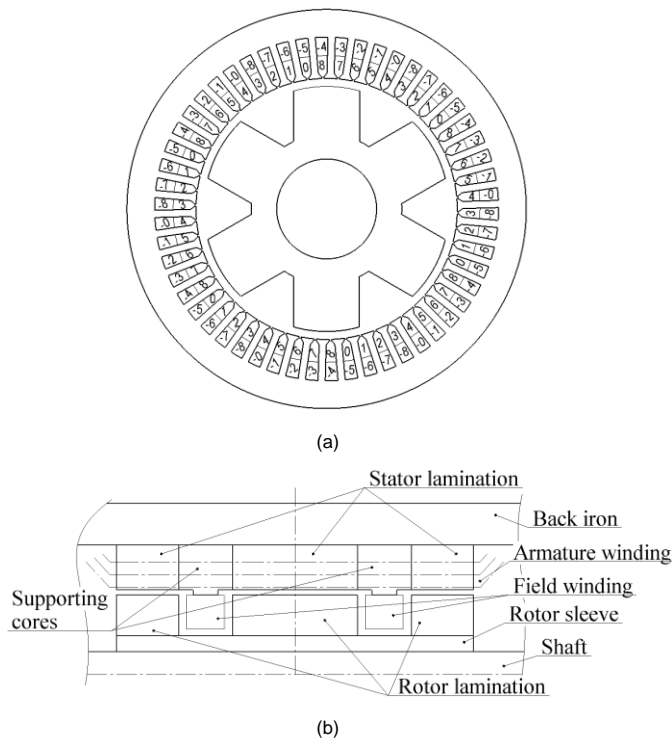


FIGURE 2. Sketch of the motor transversal (a) and axial (b) cross-sections (phases are numbered from 0 to 8).

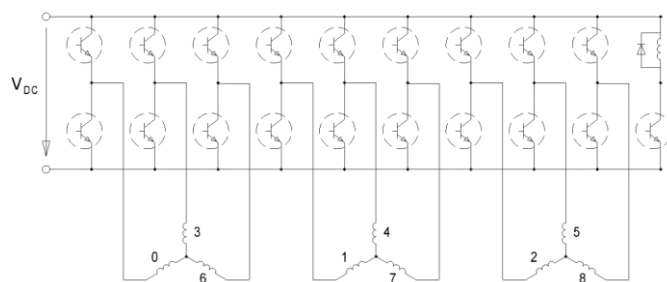


FIGURE 3. Inverter schematic.

There are two sets of SRSCs, with identical orientations of the rotor stacks. The rotor stacks of one set are rotated by 180 electrical degrees relative to the rotor stacks of another set. The total length of stacks of one set is approximately equal to the total length of the other. In the case of an SHM with three SRSCs, the first set consists of only the middle SRSC, and the second one consists of two lateral SRSCs.

These two SRSCs produce equal average torque and equal contribution to the active and reactive power in the case of sinusoidal armature currents. However, the instant values of the torque and EMF in these SRSCs are different. Therefore, the modeling of the SHM is conducted in two stages. At first, it is assumed that the SHM has only one SRSC, whose length is equal to the sum of all SRSCs' lengths. The curves of the torque, voltages, etc., are evaluated using a set of the magnetostatic problems for various rotor angular positions. Then, the symmetrization procedure should be applied to spread the results to the real SHM.

TABLE I  
MAIN PARAMETERS OF THE MOTOR

Parameter	Value
Cross-section of the stator back iron $S_{back\ iron}$ , mm <sup>2</sup>	81400
Cross-section of the rotor sleeve, mm <sup>2</sup>	78900
Outer radius of the stator stack, mm	331
Inner radius of the stator stack, mm	266
Total length of the SRSCs $a$ , mm	386
Gap between SRSCs used for a field winding $\Delta a$ , mm	73
Air gap, $\delta$ , mm	2.3
Cross-section of the rectangular armature wire, mm <sup>2</sup>	3.15 x 4.5
Number of turns in the layer, $n_w$	5
Number of strands	2
Number of parallel-connected branches, $n_{pb}$	2

### III. BOUNDARY VALUE PROBLEMS MODELING THE MAGNETIC FIELD IN THE TRANSVERSE CROSS-SECTIONS OF THE SRSC

The assumptions made for the modeling of the magnetic field in the transverse cross-sections of the SRSC is as follows:

- The magnetic field lies in the normal plane to the axis of rotation (transverse plane, further plane  $xy$ , shaft is centered to the origin)
- The current in the armature windings flows parallel to the axis of rotation

The equations of the static magnetic field are as follows:

$$\frac{\partial B_x}{\partial x} + \frac{\partial B_y}{\partial y} = 0, \quad (1)$$

$$\frac{\partial H_y}{\partial x} - \frac{\partial H_x}{\partial y} = J_z. \quad (2)$$

where  $J_z$  is the z-component of the current density, which is unequal to zero only in the slots filled with winding;  $B_x$  and  $B_y$  are the components of the magnetic flux density; and  $H_x$  and  $H_y$  are the magnetic field components.

The general solution of Gauss's law for magnetism (1) can then be expressed as follows:

$$\begin{aligned} B_x &= \frac{\partial A_z}{\partial y} + \frac{\phi x}{2\pi(x^2 + y^2)}; \\ B_y &= -\frac{\partial A_z}{\partial x} + \frac{\phi y}{2\pi(x^2 + y^2)}. \end{aligned} \quad (3)$$

The first components of these equations are conventional. The magnetic vector potential  $A$  is chosen so that only the  $A_z$  component is unequal to zero. The second parts of the equations introduce the linear density of the magnetic monopole, which simulates excitation flux. This flux flows through the shaft sleeve and stator back iron between the SRSCs and is defined as follows:

$$\Phi = \frac{a\phi}{4}, \quad (4)$$

where  $a$  is the equivalent total length of the SRSCs, and  $a/4$  is the equivalent length of the side SRSC.

Equations (2) and (3) are complemented by their constitutive equations. Consider the calculation of the current density. The current vector  $\mathbf{I}_{dq}$  in  $dq$  reference frames should be chosen as described below (23). The  $dq$  reference frames are linked to the rotor angular position and the current vector magnitude is equal to the magnitude of the phase current. For a given rotor position, the current vector  $\mathbf{I}_{xy}$  in stationary  $xy$  reference frames is evaluated. Phase currents values are evaluated using the Clarke transform generalized to the case of nine phases:

$$I_n = I_x \cos \frac{2\pi n}{n_{ph}} + I_y \sin \frac{2\pi n}{n_{ph}}. \quad (5)$$

Then, the current density is evaluated as:

$$J_z = \sum_{k=0}^{n_{ph}-1} \Xi_k I_k, \quad (6)$$

where  $\Xi_k(x, y)$  is the current density of the current equal to 1 A, which is flowing through a single phase  $k$ , when other currents are equal to zero:

$$\Xi_k(x, y) = \begin{cases} \frac{n_w}{n_{pb} S_{sec}}, & \text{when } (x, y) \in \text{phase } k \\ & \text{with positive direction of the current;} \\ -\frac{n_w}{n_{pb} S_{sec}}, & \text{when } (x, y) \in \text{phase } k \\ & \text{with negative direction of the current;} \\ 0, & \text{otherwise,} \end{cases} \quad (7)$$

where  $S_{sec}$  is the cross-section of the SRSC.

The rotor rotates together with the rotating field, and the eddy currents are mostly absent in its iron. Due to the fact that the rotor sleeve is ferromagnetic, the normal derivative of  $A_z$  is equal to zero at the inner border of the rotor stack (Neumann boundary condition).

On the contrary, magnetic field lines are frozen in the back iron of the stator and the normal component of the magnetic field at the outer boundary of the stator lamination is represented by the field of the monopole only. Therefore, the Dirichlet boundary condition  $A_z = 0$  is assumed for the outer border of the laminated stator stack.

The same computation area (see Fig. 4) is taken for the magnetostatic tasks for various rotor positions. The computation area is a sector equal to a single electrical revolution ( $360^\circ/p$ ) where an electrical revolution is equal to 60 mechanical degrees for the configuration of the rotor with 6 pole pairs in each SRSC. The computational area is divided into two subareas by the arc lying in the center of the air gap.

The boundary condition, linking magnetic vector potential at the common border of the subareas, ensures the continuity of the vector potential on both sides of the arc. The correspondence of the points on both sides of the arc depends on the rotor angular position.

A periodical boundary condition ensures the equality of the magnetic vector potential at the borders, limiting the sector of the computation area by a single electrical revolution.

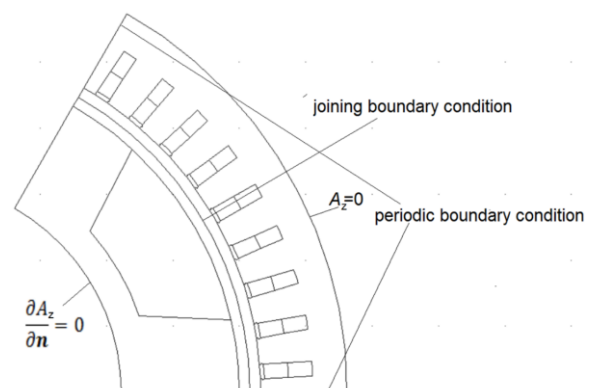


FIGURE 4. The scheme of the calculation geometry.

The SRSC is symmetric with respect to the rotor rotation by  $1/n_{ph} = 1/9$  of the electrical revolution together with the cyclic transposition of the phases. During the transposition, each phase is interchanged with the next one. Therefore, it is necessary to consider only rotor positions in the range of  $1/n_{ph}$  of the electrical revolution. This range is split into  $g$  equal parts, and  $g + 1$  boundary value problems should be solved for the following rotor positions given in electric radians:

$$\varphi_i = \frac{2\pi i}{n_{ph} g}, i = 0, 1, \dots, g. \quad (8)$$



Using the considered symmetry operation, the last boundary value problem is derived from the first when the rotor is rotated by  $1/n_{ph}$  of the electrical revolution, and it appears excessive. This additional boundary value problem is useful for the evaluation of the losses in the armature winding produced by eddy currents and for the stator or rotor core losses calculation. But it is necessary to remember that this excessive problem should be excluded when evaluating, for example, the average torque by averaging over  $g$  solutions with  $i = 0, 1, \dots, g - 1$ .

#### IV. CALCULATION OF EXCITATION MAGNETIC CIRCUIT OF THE SHM

Each field winding coil contains  $N$  turns and is located between the lamination stacks. The excitation current  $I_{exc}$  produces the magnetomotive force (MMF) as follows:

$$MMF = NI_{exc}. \quad (9)$$

The MMF drop at the SRSC for the rotor position  $i$  (8) is defined by the line integral through the computed area from the inner border of the rotor lamination stack to the outer border of the stator along the arbitrary path. Particularly, integration can be done along any radius:

$$F_i = \int_{\text{Any radius}} \frac{H_{xi}x + H_{yi}y}{r} dr, \quad (10)$$

where  $r = (x^2 + y^2)^{0.5}$  and the result of calculation of (10) for various radiuses can be different due to computational errors. Therefore, it is assumed that averaging the value of (10) over various radiuses gives more precise results. Its value is defined using the double integral over the entire computational area:

$$\begin{aligned} F_i &= \frac{p}{2\pi} \int_0^{2\pi/p} d\alpha \int \frac{H_{xi}x + H_{yi}y}{r} dr = \\ &= \frac{p}{2\pi} \iint \frac{H_{xi}x + H_{yi}y}{x^2 + y^2} dS. \end{aligned} \quad (11)$$

Since the magnetic field lines are frozen in the back iron, the linear density of the magnetic charge is assumed to be constant in time. And the MMF drop across the SRSC matches the average value (11) over all considered rotor positions (8):

$$F = \frac{p}{2\pi g} \sum_{i=0}^{g-1} \iint \frac{H_{xi}x + H_{yi}y}{x^2 + y^2} dS, \quad (12)$$

The MMF drops for the sectors of the sleeve  $F_{sleeve}$  and the back iron  $F_{back\ iron}$  are equal to:

$$F_{sleeve} = H_{sleeve} \left( \frac{\Phi}{S_{shaft}} \right) \Delta a; \quad (13)$$

$$F_{back\ iron} = H_{back\ iron} \left( \frac{\Phi}{S_{back\ iron}} \right) \Delta a, \quad (14)$$

where  $H_{sleeve}$  and  $H_{back\ iron}$  are the dependences of the magnetic field on the magnetic flux density in the sleeve and the back iron, respectively.

The equation of the excitation magnetic circuit is the following:

$$MMF = 2F + F_{back\ iron} + F_{sleeve}. \quad (15)$$

This equation (15), taking into account (4), (9), (12), (13), and (14), is an additional equation to the set of magnetostatic problems. This equation is consistent with the linear density of the magnetic charge  $\phi$ , which should be found to satisfy (15).

#### V. CALCULATION OF AVERAGED CHARACTERISTICS OF THE SHM

Though the laminations of the rotor parts are shifted by 180 electrical degrees with respect to each other, they bring the same contribution to the (average) traction torque, active and reactive powers, and losses as shown in the next section. This section considers the closed system of boundary value problems and algebraic equations for the calculations of the averaged characteristics, without taking into account the rotor lamination shift. The same assumption is convenient for the calculation of the torque waveform, voltages, and flux linkages. However, it is necessary to perform the symmetrization procedure, which is described in the next section, in order to obtain the actual waveforms.

The torque at the shaft can be calculated by integrating the Maxwellian stresses. The line integral is replaced by a double integral, which gives a higher accuracy for numerical calculations. The integral should be calculated over the cross-section of the air gap:

$$T = \frac{pa}{\delta} \iint H_{\phi} B_r r dS. \quad (16)$$

The flux linked with the phase  $n$  is calculated using:

$$\Phi_n = pa \iint \Xi_n A_z dS. \quad (17)$$

In both (16) and (17),  $p$  takes into account the reduction of the computational area.

Numerical differentiating of (17) obtains the waveform of the phase voltages, and then the phase-to-phase voltages.

The period for the torque waveform is  $1/9$  of the electrical revolution. Since the phases are connected in three three-phase systems, the spectrum of the phase-to-phase voltage is free of the triplen harmonics.

$\Phi_x$ ,  $\Phi_y$  are calculated using inverse generalized Clarke transform:

$$\begin{aligned}\Phi_x &= \frac{2}{n_{ph}} \sum_{n=0}^{n_{ph}-1} \Phi_n \cos \frac{2\pi n}{n_{ph}}, \\ \Phi_y &= \frac{2}{n_{ph}} \sum_{n=0}^{n_{ph}-1} \Phi_n \sin \frac{2\pi n}{n_{ph}}.\end{aligned}\quad (18)$$

Then  $\Phi_d$  and  $\Phi_q$  are to be calculated. Average torque can be calculated as:

$$\langle T \rangle = \frac{n_{ph} P}{2} (I_q \langle \Phi_d \rangle - I_d \langle \Phi_q \rangle), \quad (19)$$

where  $\langle \rangle$  is the averaging over  $g$  boundary value problems. Average values of torque, which are estimated using (16) and (19), are not equal due to computational errors. However, the small difference between them (of less than 0.1%) shows the correctness of the model. The average of these two values of torque estimations according to (16) and (19) is utilized for the calculation of the mechanical (active) power  $P$  excluding losses. Moreover, the reactive power  $Q$  can be evaluated as:

$$\begin{cases} P = \Omega T; \\ Q = \frac{n_{ph} \omega}{2} (I_d \langle \Phi_d \rangle + I_q \langle \Phi_q \rangle). \end{cases} \quad (20)$$

The resistance losses in the field winding  $P_{exc}$  and in the armature winding  $P_{arm}$  can be calculated using the Joule-Lenz law. Calculation of the losses in the stator  $P_{stator}$  and rotor  $P_{rotor}$  laminations can be made similar to [16]. Moreover, the eddy current losses  $P_{eddyarm}$  in the armature wires should be considered as they are induced by the slot leakage flux. The wires have a rectangular cross-section and their thickness in the normal direction to the bottom of the slot (permeated by lines of slot leakage flux) is  $h = 3.5$  mm. These losses averaged over the conductor volume for the flat conductor with the thickness of  $h$  are calculated using:

$$p_{eddy} = \frac{h^2 \sigma}{12} \left( \frac{\partial \mathbf{B}}{\partial t} \right)^2. \quad (21)$$

Taking into account the fill factor of the slot  $k_z$ , extra losses in the winding  $P_{eddyarm}$  can be calculated by integrating  $p_{eddy} k_z$  over the volume of the stator slots.

Mechanical losses are estimated using free runout experiments and they are approximated as:

$$P_{Mech.losses} = k_1 \Omega + k_3 \Omega^3, \quad (22)$$

where  $k_1 = 0.754$  W·s/rad,  $k_3 = 0.0002348$  W·s<sup>3</sup>/rad<sup>3</sup> as the friction coefficient in the ball bearings and the ventilation losses coefficient, respectively.

The losses in the stator lamination and additional losses in the armature winding are taken into account by adding a virtual current source connected in parallel to the winding. Therefore, the current vector, used in calculations  $\mathbf{I}_{dq}$  and

represented in the rotary reference frame, is expressed through the actual current vector  $\mathbf{I}_{0dq}$  as follows:

$$\mathbf{I}_{dq} = \mathbf{I}_{0dq} - \frac{2(P_{stator} + P_{EddyArm})\mathbf{U}_{dq}}{n_{ph} \mathbf{U}_{dq}^2}, \quad (23)$$

where  $\mathbf{U}_{dq}$  is the voltage vector of fundamental frequency (without considering voltage drop across phase resistance),  $U_d = -\omega \langle \Phi_q \rangle$ ,  $U_q = \omega \langle \Phi_d \rangle$  and  $\omega = 2\pi f$ .

Since the boundary value problems are non-linear, they should be solved in several iterations. In each iteration, the value of  $\mathbf{I}_{dq}$  is adjusted according to (23). Equation (23) can be considered as a recurrent equation for  $\mathbf{I}_{dq}$ . Thus, boundary value problems should be solved together with (23) and (15).

Losses in the rotor iron are considered as additional mechanical losses. Therefore, the mechanical and active powers are calculated as follows:

$$\begin{aligned}P_{mech} &= P - P_{rotor} - P_{Mech.losses}, \\ P_A &= P + P_{stator} + P_{EddyArm} + P_{arm}.\end{aligned}\quad (24)$$

Then, efficiency can be found with:

$$\eta = \frac{P_{mech}}{P_A + P_{exc}}. \quad (25)$$

## VI. SYMMETRIZATION

This section considers the shift of the SRSC by 180 electrical degrees, which helps calculate actual waveforms of the torque and voltages based on the waveforms of torque and voltages obtained in the previous section.

Two adjacent SRSCs have the following traits: 1) the phase current is the same in both SRSCs due to the fact that it is formed by the same parts of coils lying in the stator slots; 2) the drop of excitation MMF is opposite in them; and 3) the rotor stacks are shifted by 180 electrical degrees.

The processes in each SRSC are symmetric with respect to simultaneous changing signs of excitation MMF and currents, wherein, the EMF induced in the stator slots also changes its sign. Upon applying the symmetry operation to the second SRSC, the following properties will be obtained: 1) the phase current is shifted by 180 degrees (due to the change of the sinusoidal current signs); 2) the MMF drop is coincidental with the first SRSC; and 3) the rotor stacks are shifted by 180 electrical degrees.

In other words, the operation of symmetry reflects the processes in the second SRSC into processes in the first SRSC with the shift of 180 degrees. As mentioned above, there are two SRSC sets of equal length which produce equal average torque. Thus, the torque of the second SRSC set is equal to the torque of the first SRSC set with a shift of 180 degrees, while the voltages have opposite signs. Therefore, after the calculation of the torque and voltage waveforms, supposing that the motor contains only one SRSC of the total length of three SRSCs, symmetrization must be performed:

$$\begin{aligned} T_{sym} &= \left( T(t) + T\left(t + \frac{\tau}{2}\right) \right) / 2; \\ U_{sym} &= \left( U(t) - U\left(t + \frac{\tau}{2}\right) \right) / 2. \end{aligned} \quad (26)$$

where  $U$  and  $T$  are the phase voltage and the torque before the symmetrization and  $\tau$  is the electrical period.

No limitations to the number of parts  $g$  of the interval of the considered rotor positions were specified till now. Now, this number  $g$  should be even. Then, the shift by half of the electrical revolution can be performed by adding  $g/2$  to the index of the data arrays (the next element for the last element is assumed to be the first element). However, phase voltage cannot be measured for the motors which have no neutral point. The waveform of the phase-to-phase voltage is evaluated using the following equation:

$$U_{line} = U_{sym}(t) - U_{sym}\left(t + \frac{2\tau}{3}\right). \quad (27)$$

Therefore, it is better to take  $g$  in multiples of 2 and 3, or multiples of 6. Then, the shift by  $2/3$  of the electrical revolution is done by adding  $2g/3$  to the index of the data arrays. The torque period was reduced from  $1/9$  to  $1/18$  as a result of the symmetrization procedure. Moreover, not only triplen voltage harmonics are unobservable, but even voltage harmonics are unobservable as well. Thus, the existing harmonics are  $6l + 1$ , where  $l$  is the integer number.

## VII. COMPUTATION AND EXPERIMENTAL RESULTS

Two experimental prototypes of the considered motor design were tested using the dual supply back-to-back method (2-1-1D method according to IEC 60034-2-1-2014). Fig. 5 shows the SHM prototype used in the experiments and its rotor is shown in Fig. 6. One of the SHMs operates in the braking (generator) mode, creating the load for another SHM operating in the motor mode. The inverters of both machines which schematic is shown in Fig.3 were connected to the common DC-link. As a result, the power consumed from DC-link is equal only to the total losses in the SHMs and in the inverters. The machines were tested with external air cooling. Fig. 7 shows the testbench with the two traction SHMs and two inverters of the powertrain of a mining truck.

The electrical power of both SHMs is measured using the power analyzer. The difference between the active motor power and the active generator power is the sum of the power losses in two identical machines operating at the same rotational speed and producing the same torque. Assuming that the losses in both SHMs are the same, the total losses in each can be calculated as well as the mechanical shaft power.

Table II demonstrates some operation modes of the SHM observed in the experiment. The excitation current, the armature winding current and the current angle in these modes were used to carry out the computations. The

computation results are also provided in the Table II for the comparison.

The speeds in the last three modes are approximately equal. The efficiency and the torque ripple are approximately equal in these three modes, which shows that it is possible to adjust operation conditions to avoid the voltage or current limit. Namely, depending on excitation current, the armature winding current takes the values from 253 A ampl., to 286 A ampl.

The symmetrization procedure is needed to compute the waveforms of the torque and the voltages. Table II shows that the torque ripple of the SHM (after the symmetrization) is more than thrice as less than the torque ripple of the single SRSC (before the symmetrization).

TABLE II  
OPERATION MODE PARAMETERS OF THE SHM

Mode Number	1	2	3	4	5
Speed, rpm	3102	2440	1443	1420	1400
Armature current, A, ampl.	174	195	253	286	271
Excitation current, A	5.6	6.4	9.2	7.6	9
Control angle, el. Degrees	24	15	0	0	0
Active power, W	329.1	340.2	332.0	325.7	339.0
Torque ripple before symmetrization, %	69.4	69.8	66.9	67.7	66.5
Torque ripple after symmetrization, %	22.2	19.3	15.1	14.7	14.7
Mechanical losses, kW	8.29	4.11	0.92	0.88	0.85
Resistance armature winding losses, kW	1.46	1.84	3.09	3.95	3.54
Eddy-current armature winding losses, kW	2.84	2.56	2.12	2.02	2.13
Excitation winding losses, kW	0.39	0.51	1.06	0.72	1.01
Mechanical losses, kW	8.29	4.11	0.92	0.88	0.85
Stator core losses, kW	10.41	9.57	7.08	6.62	6.82
Rotor core losses, kW	1.95	1.75	1.10	0.90	1.01
Computed motor efficiency, %	92.3	94.0	95.4	95.4	95.5
Power factor (under the first harmonic)	0.985	0.962	0.923	0.852	0.907
Computed efficiency of the inverter, %	97.4	97.2	96.9	96.8	96.8
Computed efficiency of the drive including inverter and motor, %	89.9	91.4	92.4	92.3	92.4
Measured efficiency of the drive including inverter and motor, %	89.7	92.3	91.6	91.6	90.8
Motor mechanical power, kW (computed)	304.1	320.4	317.7	311.3	324.6
Motor mechanical power, kW (experimental)	324.7	332.0	324.7	322.5	319.4

Table II also represents the experimental and calculated efficiency of the SHM drive (efficiency of the inverter and the motor). Besides, comparison of the computed an experimental motor mechanical power is provided in Table II. The experimental SHM mechanical power differs



from the computed one by less than 7%. The difference between the computed and experimental efficiencies of the drive (including the convertor and the SHM) is less than 1.6%. The developed mathematical model can be used in designing SHMs.

The power factor under the first (fundamental) harmonic is also provided in Table II. It can be rather high at proper adjusting the control angle and the excitation current.

The eddy-current losses in the armature winding are comparable with its resistance losses and grow with the growth of the motor speed, which should be taken into account during thermal calculations of the winding behavior.



**FIGURE 5.** SHM experimental prototype.



**FIGURE 6.** Rotor of the experimental prototype.

The considered SHMs have passed tests as a part of the powertrain of a mining truck having two rear driving wheels. It is hybrid electric mining truck BELAZ 75570 carrying 90 tons (Fig. 8).

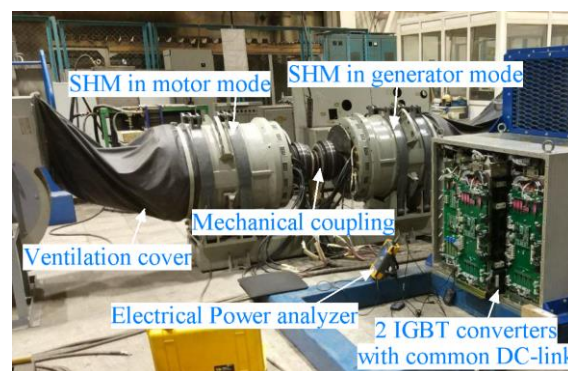


**FIGURE 7.** Testing the motor prototypes.



**FIGURE 8.** The mining truck with two SHMs as rear-wheel motors.

Two SHMs were used as rear-wheel motors of mining truck BELAZ 75570 to replace induction motors (IM) used earlier. The SHMs have identical dimensions and specific characteristics as the IMs. The identical forced-air cooling systems with the same power consumption are used for the SHMs and IMs. The main advantage of traction SHMs over traction IMs is their high reliability. A more detailed comparison of SHM with other traction motors for the mining truck will be done in further papers.

## VII. CONCLUSION

In this paper, a novel 2D FEM of the SHM is proposed. The FEM uses the general solution of the Gauss's law for magnetism containing the excitation flux represented by the magnetic monopole field. Since the magnetic monopole is located outside the computation area, the computation area does not contain any imaginary elements distorting the magnetic field picture. The symmetry between electromagnetic processes in neighboring stator rotor stack combinations (SRSCs) is investigated in the paper, which allows predicting the torque and voltage waveforms of the whole motor by computing those for a single SRSC. The SRSC symmetry also is studied to reduce the computation area and to determine the necessary range of rotor position to be considered. The model is based on a set of magnetostatic boundary value problems for various rotor positions, solved with the finite element method. The set of boundary problems is completed with the excitation equivalent circuit.



The losses in the armature and field windings, as well as in the stator and rotor magnetic cores are computed in postprocessing.

A comparison of the theoretical and experimental data for nine-phase three-section 320 kW SHM is carried out. These SHMs were used as rear-wheel motors in a mining truck with the carrying capacity of 90 tons. A high reliability of the proposed SHM was validated during its two-year operation as part of the powertrain of the electric mining truck. As a result, the proposed SHMs can be recommended for replacing traction induction motors in hybrid electric mining vehicles of this kind.

## REFERENCES

- [1] C. Ye, J. Yang, F. Xiong and Z. Q. Zhu, "Relationship Between Homopolar Inductor Machine and Wound-Field Synchronous Machine," in *IEEE Transactions on Industrial Electronics*, vol. 67, no. 2, pp. 919-930, Feb. 2020, doi: 10.1109/TIE.2019.2898577.
- [2] G. R. Bindu, J. Basheer and A. Venugopal, "Analysis and control of rotor eccentricity in a train-lighting alternator," 2017 *IEEE International Conference on Power, Control, Signals and Instrumentation Engineering (ICPCSI)*, Chennai, 2017, pp. 2021-2025, doi: 10.1109/ICPCSI.2017.8392070.
- [3] C. Bianchini, F. Immovilli, A. Bellini, E. Lorenzani, C. Concarì and M. Scolari, "Homopolar generators: An overview," 2011 *IEEE Energy Conversion Congress and Exposition*, Phoenix, AZ, 2011, pp. 1523-1527, doi.org/10.1109/ECCE.2011.6063962.
- [4] K. Yu, J. Yao, X. Xie and P. Tang, "A Novel Critical Analysis Method of Homopolar Inductor Alternator for Preliminary Design in Capacitor Charge Power Supply," in *IEEE Transactions on Plasma Science*, vol. 47, no. 5, pp. 2354-2361, May 2019, doi: 10.1109/TPS.2019.2892610.
- [5] E. Severson, R. Nilssen, T. Undeland and N. Mohan, "Magnetic Equivalent Circuit Modeling of the AC Homopolar Machine for Flywheel Energy Storage," in *IEEE Transactions on Energy Conversion*, vol. 30, no. 4, pp. 1670-1678, Dec. 2015, doi: 10.1109/TEC.2015.2441040.
- [6] M. Lashkevich, A. Anuchin, D. Aliamkin and F. Briz, "Control strategy for synchronous homopolar motor in traction applications," *IECON 2017 - 43rd Annual Conference of the IEEE Industrial Electronics Society*, Beijing, 2017, pp. 6607-6611, doi: 10.1109/IECON.2017.8217153.
- [7] N. Sugitani, A. Chiba and T. Fukao, "Characteristics of a doubly salient-pole homopolar machine in a constant-power speed range," *Conference Record of 1998 IEEE Industry Applications Conference. Thirty-Third IAS Annual Meeting (Cat. No.98CH36242)*, St. Louis, MO, USA, 1998, pp. 663-670 vol.1, doi: 10.1109/IAS.1998.732399.
- [8] S. Lee, J. Hong, Y. Kwon, Y. Jo and S. Baik, "Study on Homopolar Superconductivity Synchronous Motors for Ship Propulsion Applications," in *IEEE Transactions on Applied Superconductivity*, vol. 18, no. 2, pp. 717-720, June 2008, doi: 10.1109/TASC.2008.921334.
- [9] E. Severson, R. Nilssen, T. Undeland and N. Mohan, "Dual-Purpose No-Voltage Winding Design for the Bearingless AC Homopolar and Consequent Pole Motors," in *IEEE Transactions on Industry Applications*, vol. 51, no. 4, pp. 2884-2895, July-Aug. 2015, doi: 10.1109/TIA.2015.2388852.
- [10] J. Jeong, D. An, J. Hong, H. Kim and Y. Jo, "Design of a 10-MW-Class HTS Homopolar Generator for Wind Turbines," in *IEEE Transactions on Applied Superconductivity*, vol. 27, no. 4, pp. 1-4, June 2017, Art no. 5202804, doi: 10.1109/TASC.2017.2669140.
- [11] H. M. Cheshmehbeigi and E. Afjei, "Design Optimization of a Homopolar Salient-Pole Brushless DC Machine: Analysis, Simulation, and Experimental Tests," in *IEEE Transactions on Energy Conversion*, vol. 28, no. 2, pp. 289-297, June 2013, doi: 10.1109/TEC.2013.2249584.
- [12] E. Severson, R. Nilssen, T. Undeland and N. Mohan, "Outer-rotor ac homopolar motors for flywheel energy storage," 7th *IET International*

Conference on Power Electronics, Machines and Drives (PEMD 2014), Manchester, 2014, pp. 1-6, doi: 10.1049/cp.2014.0345.

- [13] J. Yang et al., "Investigation of a Two-Dimensional Analytical Model of the Homopolar Inductor Alternator," in *IEEE Transactions on Applied Superconductivity*, vol. 28, no. 3, pp. 1-5, April 2018, Art no. 5205205, doi: 10.1109/TASC.2018.2802480.
- [14] Q. Wang, C. Liu, J. Zou, X. Fu and J. Zhang, "Numerical Analysis and Design Optimization of a Homopolar Inductor Machine Used for Flywheel Energy Storage," in *IEEE Transactions on Plasma Science*, vol. 41, no. 5, pp. 1290-1294, May 2013, doi: 10.1109/TPS.2013.2243847.
- [15] C. Belalahy, I. Rasoanarivo and F. M. Sargos, "Using 3D reluctance network for design a three phase synchronous homopolar machine," 2008 34th Annual Conference of IEEE Industrial Electronics, Orlando, FL, 2008, pp. 2067-2072, doi: 10.1109/IECON.2008.4758275.
- [16] V. Dmitrievskii, V. Prakht, V. Kazakbaev, S. Oshurbekov and I. Sokolov, "Developing ultra premium efficiency (IE5 class) magnet-free synchronous reluctance motor," 2016 6th International Electric Drives Production Conference (EDPC), Nuremberg, 2016, pp. 2-7, doi: 10.1109/EDPC.2016.7851306.



**VLADIMIR DMITRIEVSKII** received the master's degree in theoretical physics and the Ph.D. degree from Ural Federal University, Yekaterinburg, Russia, in 1996 and 2007, respectively. He submitted his Ph.D.

dissertation on mathematical modeling and optimal designing the linear electric motors in 2006. He is an Associate Professor with the Department of Electrical Engineering, Ural Federal University. His research interests include optimal designing energy efficient motors and developing sensorless control algorithms for electric drives.



**VLADIMIR PRAKHT** received the graduate degree in engineering and the Ph.D. degree from the Department of Electrical Engineering, Ural Federal University, Yekaterinburg, Russia, in 2004 and 2007, respectively. He submitted his Ph.D. dissertation on optimal control and mathematical modeling induction heating systems in 2006. He is an Associate Professor with the Department of Electrical Engineering, Ural Federal University. His research interests include mathematical modeling and optimal

design of energy efficient electric motors and generators.



**ALECKSEY ANUCHIN** received the B.Sc., M.Sc., Ph.D., and Dr.Eng.Sc. degrees from Moscow Power Engineering Institute, Moscow, Russia, in 1999, 2001, 2004, and 2018, respectively. He delivers lectures on "control systems of electric drives," "real-time software design," "electric drives," and "science research writing" at Moscow Power Engineering Institute. He has been in a head position with the Electric Drives Department for the last eight years. He has more than 20 years of experience

covering control systems of electric drives, hybrid powertrains, and real-time communications. He is the author of three textbooks on the design of real-time software for the microcontroller of the C28 family and Cortex-M4F, and control system of electric drives (in Russian). He has authored or coauthored more than 100 conference and journal papers.



**VADIM KAZAKBAEV** received the graduate degree in engineering and the Ph.D. degree from the Department of Electrical Machines, Ural Federal University, Yekaterinburg, Russia, in 2010 and 2017, respectively. He submitted his Ph.D. dissertation on “Development of High-Performance Synchronous Reluctance Motor” in 2016. He is a Junior Researcher and an Associate Professor with the Department of Electrical Engineering, Ural Federal University. His research interests include electrical engineering, design of electrical machines, and control of electrical drives.